Enhanced trapped field performance of bulk high-temperature superconductors using split coil, pulsed field magnetization with an iron yoke

M D Ainslie[1], H Fujishiro[2], H Mochizuki[2], K Takahashi[2], Y-H Shi[1], D K Namburi[1], J Zou[1], D Zhou[1], A R Dennis[1] and D A Cardwell[1]

[1]Bulk Superconductivity Group, Department of Engineering, University of Cambridge, Trumpington Street, Cambridge CB2 1PZ, UK
[2]Department of Materials Science and Engineering, Faculty of Engineering, Iwate University, 4-3-5 Ueda, Morioka 020-8551, Japan

Abstract

Investigating and predicting the magnetization of bulk superconducting materials and developing practical magnetizing techniques is crucial to using them as trapped field magnets (TFMs) in engineering applications. The pulsed field magnetization (PFM) technique is considered to be a compact, mobile and relative inexpensive way to magnetize bulk samples, requiring shorter magnetization times (on the order of milliseconds) and a smaller and less complicated magnetization fixture; however, the trapped field produced by PFM is generally much smaller than that of slower zero field cooling (ZFC) or field cooling (FC) techniques, particularly at lower operating temperatures. In this paper, the PFM of two, standard Ag-containing Gd-Ba-Cu-O samples is carried out using two types of magnetizing coils: 1) a solenoid coil, and 2) a split coil, both of which make use of an iron yoke to enhance the trapped magnetic field. It is shown that a significantly higher trapped field can be achieved using a split coil with an iron yoke, and in order to explain these how this arrangement works in detail, numerical simulations using a 2D axisymmetric finite element method based on the ***H***-formulation are carried to qualitatively reproduce and analyse the magnetization process from both electromagnetic and thermal points of view. It is observed that after the pulse peak significantly less flux exits the bulk when the iron core is present, resulting in a higher peak trapped field, as well as more overall trapped flux, after the magnetization process is complete. The results have important implications for practical applications of bulk superconductors as such a split coil arrangement with an iron yoke could be incorporated into the design of a portable, high magnetic field source/magnet to enhance the available magnetic field or in an axial gap-type bulk superconducting electric machine, where iron can be incorporated into the stator windings to 1) improve the trapped field from the magnetization process, and 2) increase the effective air-gap magnetic field.

1. Introduction

Bulk superconductors, acting as trapped field magnets (TFMs), can trap magnetic fields of magnitude over ten times higher than the maximum field produced by conventional magnets, which is limited practically to rather less than 2 T [1]. Indeed, it has been shown that (RE)BCO (where RE= rare earth or Y) bulk superconductors can trap fields greater than 17 T – the longstanding world record field generated by an arrangement of two bulk superconductors of 17.24 T at 29 K [2] was recently exceeded by 17.6 T at 26 K in [3]. Additionally, bulk superconductors can exhibit critical current densities, J_cs, of 5 x 10^4 Acm^{-2} at 1 T and 77 K, resulting in typical trapped fields of up to between 1 – 1.5 T for Y-Ba-Cu-O (YBCO) and greater than 2 T for (RE)BCO at this technologically important temperature, with 3 T the highest trapped field at 77 K so far [4]. As a result, there is great interest in using these materials as TFMs in a number of engineering applications, including magnetic bearings, energy storage flywheels, magnetic resonance imaging, magnetic separation and rotating machines [5-7]. Significantly, the higher magnetic loading in rotating machines would provide an increased torque/power density, resulting potentially in a machine that is smaller and lighter in weight than conventional devices of the same rating [8-11].

Investigating and predicting the magnetization of these technologically important materials and developing practical magnetizing techniques is crucial to using them as TFMs in applications of these types. The pulsed field magnetization (PFM) technique is considered to be a compact, mobile and relative inexpensive way to magnetize bulk samples, requiring shorter magnetization times (on the order of milliseconds) and a smaller and less complicated magnetization fixture; however, the trapped field produced by PFM is generally much smaller than that of slower zero field cooling (ZFC) or field cooling (FC) techniques, particularly at lower operating temperatures, due to the large temperature rise ΔT associated with the rapid dynamic movement of the magnetic flux in the interior of the superconductor during the PFM process [12]. Accordingly, the record trapped field produced so far by PFM is only 5.2 T at 29 K [13].

There are many considerations and variables for the PFM technique, including the duration, magnitude and shape of the pulse, the number of pulses, the temperature(s) at which the pulse(s) is applied, and the shape and type of the magnetizing coil(s) [12]. In this paper, the last of these considerations is investigated in detail and the PFM of two, standard Ag-containing Gd-Ba-Cu-O samples – of the same composition that recently achieved the new record trapped field [3] – is carried out using two types of magnetizing coils: 1) a solenoid coil, and 2) a split coil, both of which make use of an iron yoke to enhance the trapped magnetic field. Bulk superconductors are often used in applications that incorporate ferromagnetic materials, such as in motors and generators [14, 15]. Ferromagnets can also increase the force in levitation systems [16, 17], and can improve the available flux produced by bulk superconductors [18-22].

The trapped field performance and magnetic flux dynamics of the samples for these two coil arrangements are compared experimentally, and these configurations are then modelled using a 2D axisymmetric finite element method based on the ***H***-formulation to qualitatively reproduce and analyse the magnetization process from both electromagnetic and thermal points of view. It is shown that using a split coil arrangement with an iron yoke results in an enhanced trapped field performance for pulsed fields of equivalent duration, magnitude and shape, chiefly because the iron yoke acts to attract flux to remain in the bulk after the pulse peak.

2. Sample Processing Details

For this study, two cylindrical Ag-containing (15 wt%) Gd-Ba-Cu-O (GdBCO) bulk samples of 30 mm in diameter and 15 mm in thickness were grown using the top-seeded melt growth (TSMG) process described elsewhere [23]. We have previously developed Ag-containing GdBCO samples that exhibit good field-trapping performance at 77 K [23] and have shown record trapped field capabilities, greater than 17 T, below 30 K in a stack of two such samples [3]. No significant deleterious effect on J_c has been observed for an Ag content of up to 15 wt% AgO_2, and they exhibit a more homogenous J_c distribution than TSMG-processed Y-Ba-Cu-O (YBCO) samples [24].

3. Field Cooling Magnetization

The FC magnetization technique gives the best indication of the trapped field capability of a bulk superconductor sample and is useful for comparing the maximum potential of different samples [25, 26]. Fig. 1 shows the FC results for the two samples, measured by a Hall sensor placed at the centre of the top surface of the sample, as the temperature is increased slowly from 40 to 100 K after application of a 7 T magnetic field. The two samples achieved trapped field values of B_t = 6 T (#476) and 5.44 T (#477) at 40 K and B_t = 3.11 T (#476) and 2.02 T (#477) at 65 K. The two-dimensional (2D) trapped field distributions at 77 K obtained by FC are also shown for each sample in Figure 2, measured approximately 1 mm above the top surface using a scanning system consisting of a linear array of Hall probes [27].

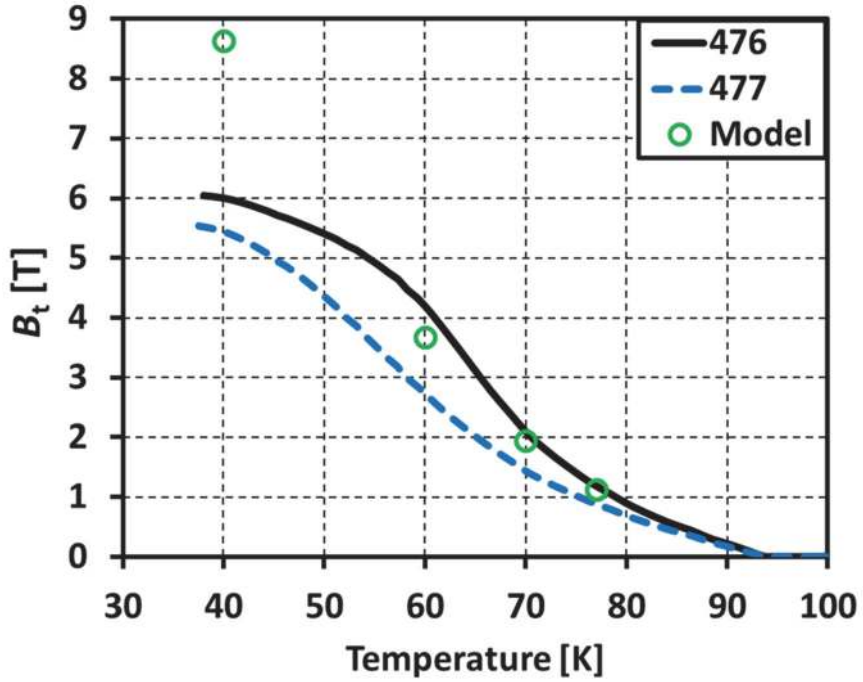

Figure 1. Field cooling (FC) magnetization results for the two Ag-containing GdBCO samples, measured at the centre of the top surface of each sample, with an external applied field of 7 T.

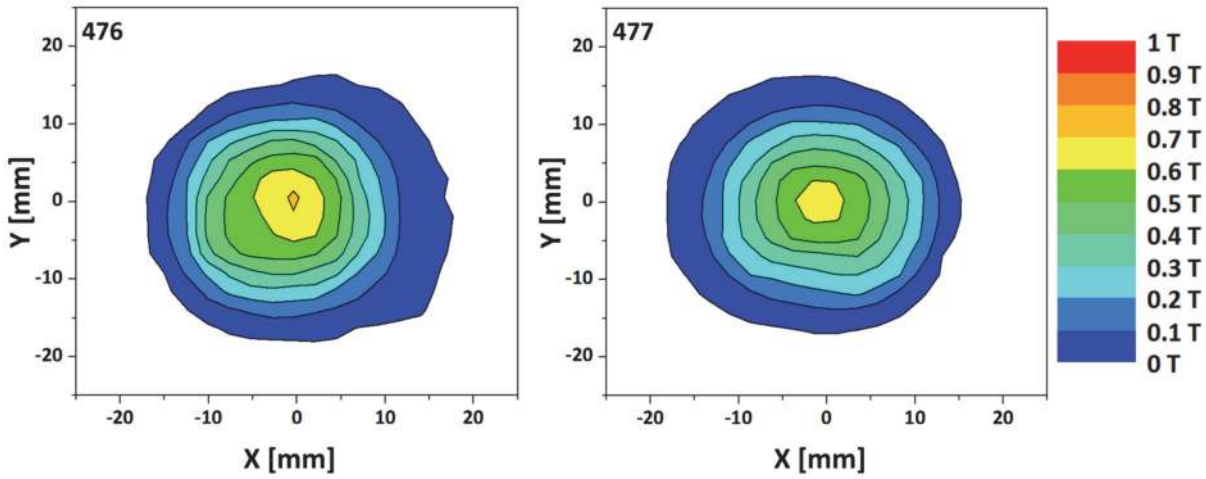

Figure 2. Trapped field distributions for each sample, obtained by field cooling (FC) magnetization at 77 K in an external magnetic field of 1.5 T and measured approximately 1 mm above the top surface using a scanning system consisting of a linear array of Hall probes.

4. Pulsed Field Magnetization

4.1 Split Coil Experimental Setup

Figure 3 shows a schematic diagram (top) and photograph (bottom) of the sample holder for the PFM experiments using the split coil arrangement. To ensure a good thermal contact between the samples and the copper sample holder, a thin ring of indium (of approx. 0.2 mm thickness) is placed around the periphery of each sample. A heater is used to regulate the operating temperature, which is measured using a Pt-Co thermometer. The sample holder is connected to the cold stage of a Gifford–McMahon (GM) cycle helium refrigerator in the vacuum chamber, which has a small vacuum space of 1 mm. A Hall sensor was adhered on the bulk surface to measure the magnetic field dynamically during the experiments. A split-type coil with an inner diameter (ID) 72 mm, outer diameter (OD) of 124 mm, and height of 35 mm, which was submerged in liquid nitrogen, was placed outside the vacuum chamber as the magnetizing fixture, and a pair of soft iron yokes (60 mm in diameter and 65 in height) were inserted in the hole of the split-type coil. This geometry and experimental setup, including sample mounting, is shown in Figure 4. The initial temperature, T_{op}, of the bulk was set to 65 and 40 K. Magnetic pulses, B_{ex}, up to around 6 T, with a rise time of t_r = 18 ms and duration of approximately t_d = 200 ms were applied via a pulse current in the coil. The typical evolution of the applied pulsed fields from this arrangement, as measured by the current flowing through a shunt resistor, is shown in Figure 5. After the removal of the split coil, the two-dimensional trapped field distributions were measured on the outside surface of the vacuum chamber, at a distance approximately 2 mm above the bulk surface by scanning a Hall sensor using an x–y stage controller.

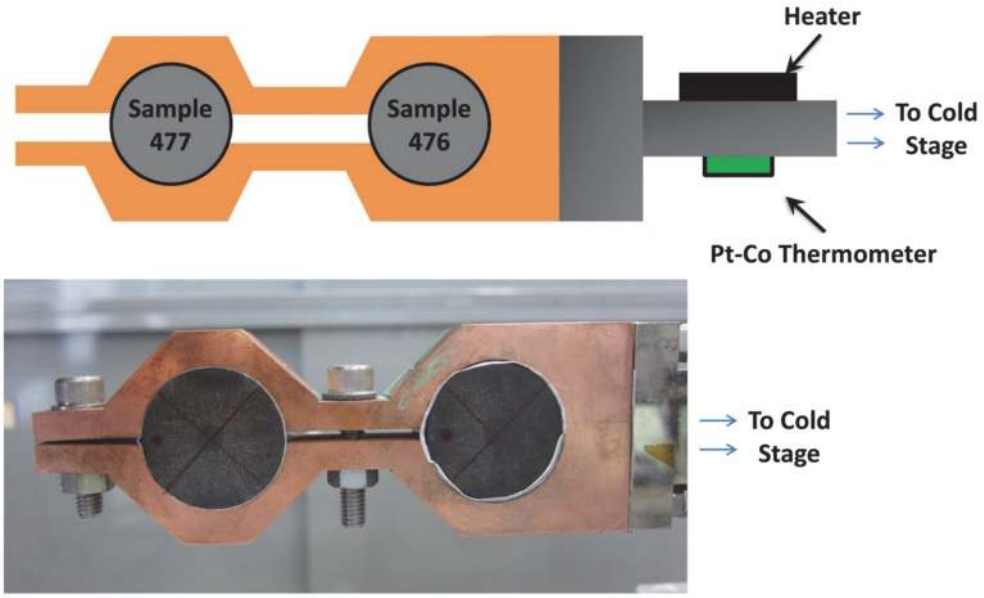

Figure 3. Schematic diagram (top) and photograph (bottom) of the sample holder for PFM experiments using the split coil arrangement. To ensure a good thermal contact between

the samples and the sample holder, a thin ring of indium is placed around the periphery of each sample. A heater is used to regulate the operating temperature, which is measured using a Pt-Co thermometer.

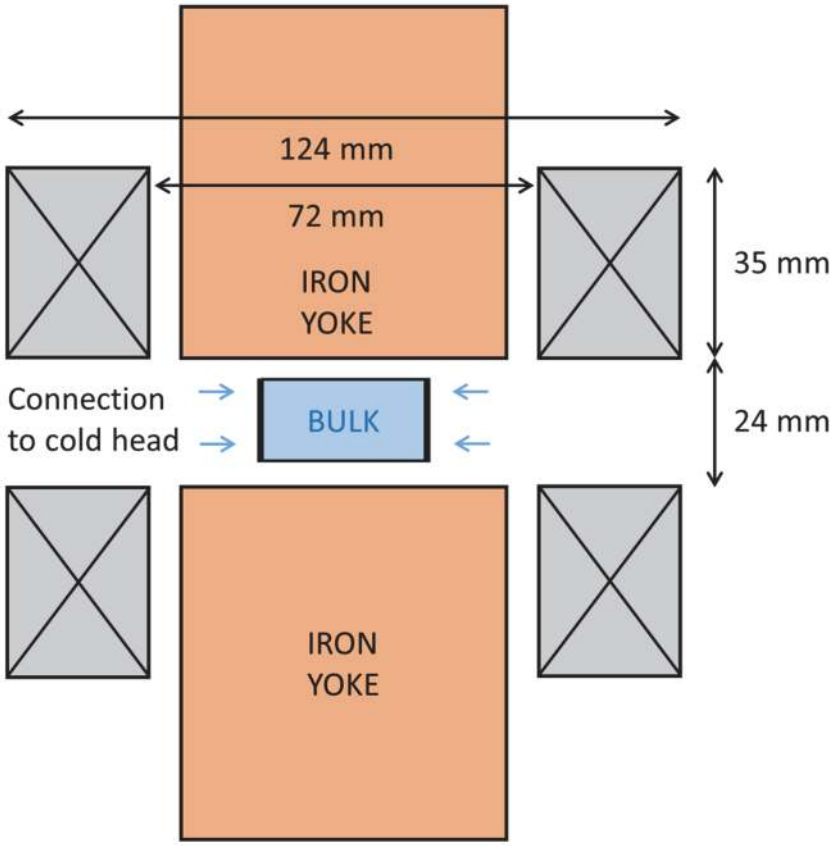

Figure 4. Geometry and experimental setup, including sample mounting, for pulsed field magnetization using a split coil with an iron yoke.

4.2 Solenoid Coil Experimental Setup

An overview of the pulsed field magnetization experimental setup using a solenoid coil is described in [24]. The bulk samples were mounted tightly on a sample holder fabricated from 316 stainless steel of inner diameter slightly larger than the diameter of the samples and outer diameter 56 mm to match the dimensions of the available cold stage of the pulse system. Stycast™ was used to mount the samples in the holder, which was then mounted on the cold stage of a Gifford-McMahon (GM), closed cycle helium refrigerator, and a copper magnetizing solenoid pulse coil, cooled using liquid nitrogen, was placed outside the vacuum chamber. The direction of external applied field is parallel to the c-axis of the bulk samples. The magnetizing coil can provide pulsed external fields up to B_{app} = 6.4 T with a rise time of t_r = 12 ms and duration of approximately t_d = 120 ms [24]. The typical evolution of

the applied pulsed fields from this arrangement, as measured by the current flowing through a shunt resistor, is shown in Figure 5. After PFM of the sample using the solenoid coil, the two-dimensional trapped field distributions were measured inside the vacuum chamber using an x-y stage controller and an axial-type Hall sensor positioned 2 mm above the top surface of the samples. The trapped field close to the centre of the top surface of the samples was measured dynamically during the application of each pulsed field using the same Hall sensor.

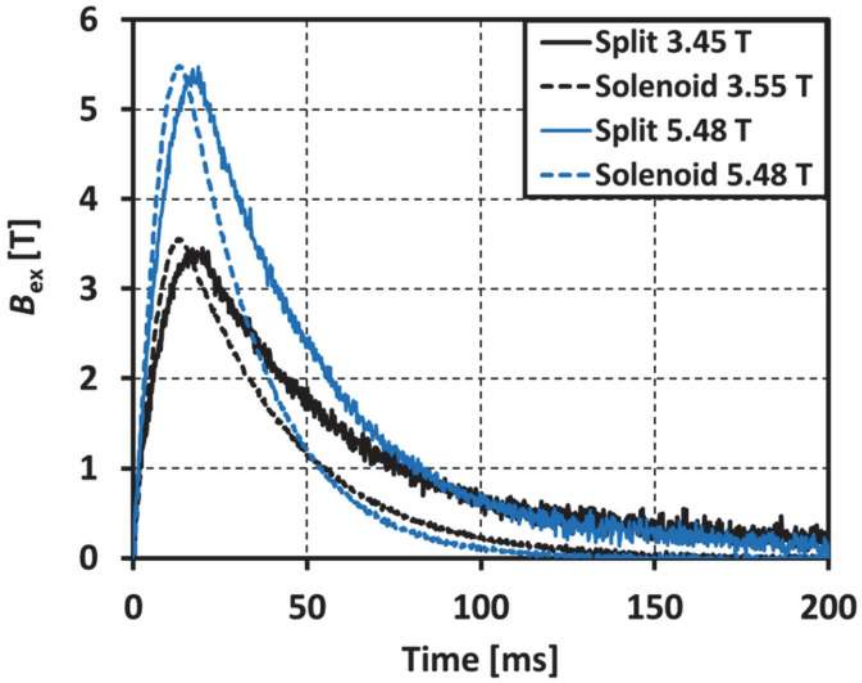

Figure 5. Typical evolution of the applied pulsed fields with time, estimated from the measured current flowing through a shunt resistor for the split and solenoid coils with an iron yoke.

4.3 Pulsed Field Magnetization Results

Figures 6 and 7 show a comparison of the measured trapped fields (at approx. t = 300 ms) after activation by PFM using the split coil (solid lines) and the solenoid coil (dashed lines) at operating temperatures of 65 K and 40 K, measured at the centre of the top bulk surface, for samples #476 and #477, respectively. It is clear that for both samples, the split coil arrangement results in a significantly larger measured trapped field, and at 40 K in particular, not only is the trapped field significantly larger, but the activation field (defined as the field required to fully magnetize the bulk sample [24]) is reduced in comparison to the solenoid coil. The lower activation field for the #477 sample (Figure 7) and its lower trapped field by FC magnetization suggests that the overall J_c is lower in comparison to sample #476.

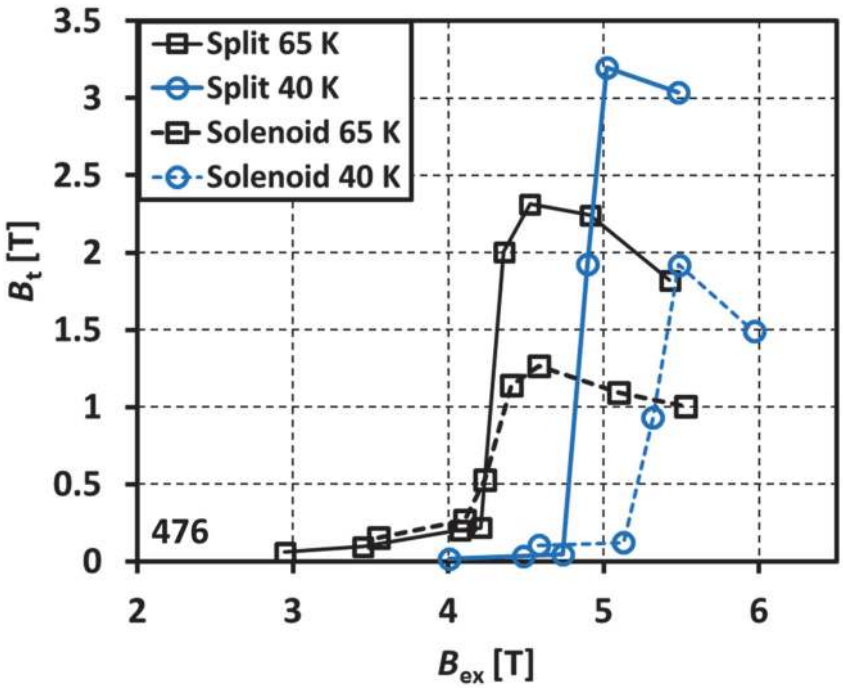

Figure 6. Comparison of trapped fields for sample #476 after activation by PFM using the split coil (solid lines) and the solenoid coil (dashed lines) at operating temperatures of 65 K and 40 K, measured at the centre of the top bulk surface.

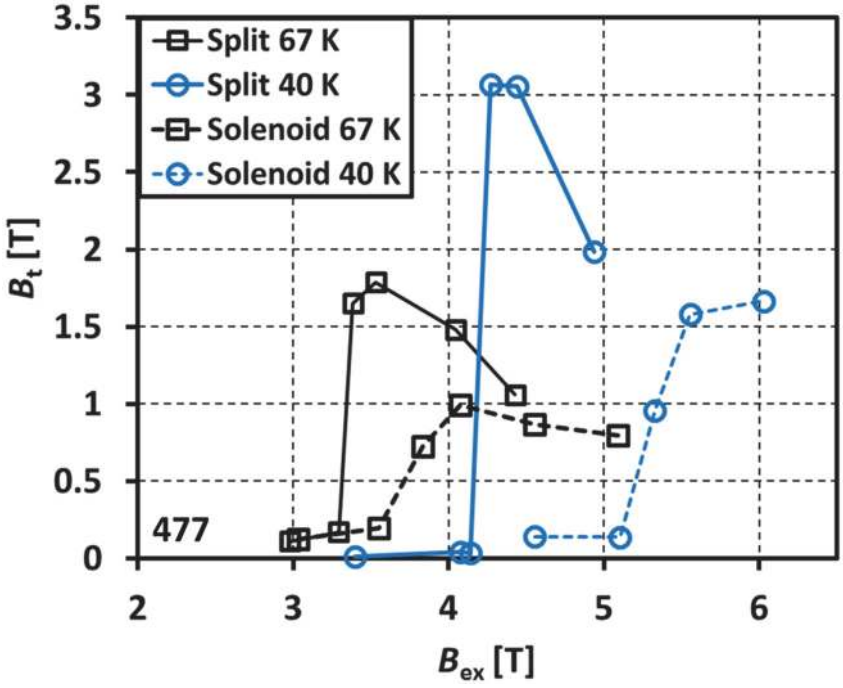

Figure 7. Comparison of trapped fields for sample #477 after activation by PFM using the split coil (solid lines) and the solenoid coil (dashed lines) at operating temperatures of 65 K and 40 K, measured at the centre of the top bulk surface.

Figures 8 and 9 show the 2D trapped field surface plots for sample #476 measured at 65 K when magnetized by the split coil (Figure 8) and solenoid coil (Figure 9), and Figures 10 (split) and 11 (solenoid) show the same plots for the same sample measured at 40 K. The 2D surface plots were taken using the scanning system approximately t = 20 mins after the application of the pulse, and in the case of the split coil measurement, the scanning measurement took place after the split coil (and iron yoke) were moved well away from the sample (in the case of the solenoid coil arrangement, the iron yoke is still present after magnetization and for the scanning measurement since it is embedded in the magnetizing fixture). Hence, there is a reduction in the observed peak trapped field, but the magnitude is still higher in the case of the split coil: B_t (65 K) ≈ 1.2 T (split), B_t (65 K) ≈ 0.9 T (solenoid); B_t (40 K) ≈ 1.8 T (split), B_t (40 K) ≈ 1.3 T (solenoid). The surface plots show that the magnetic flux penetrates into both samples in a fairly uniform manner, similar to the results for the GdBCO sample presented in [24], which suggests a homogeneous J_c distribution around the *ab*-plane of the samples.

In order to fully understand the mechanism(s) by which the split coil with an iron yoke acts to enhance the trapped field, a numerical model is developed in the following section to analyse the electromagnetic and thermal properties of the bulk during each magnetization process, and thoroughly investigate the positive effect an iron yoke has on the trapped field.

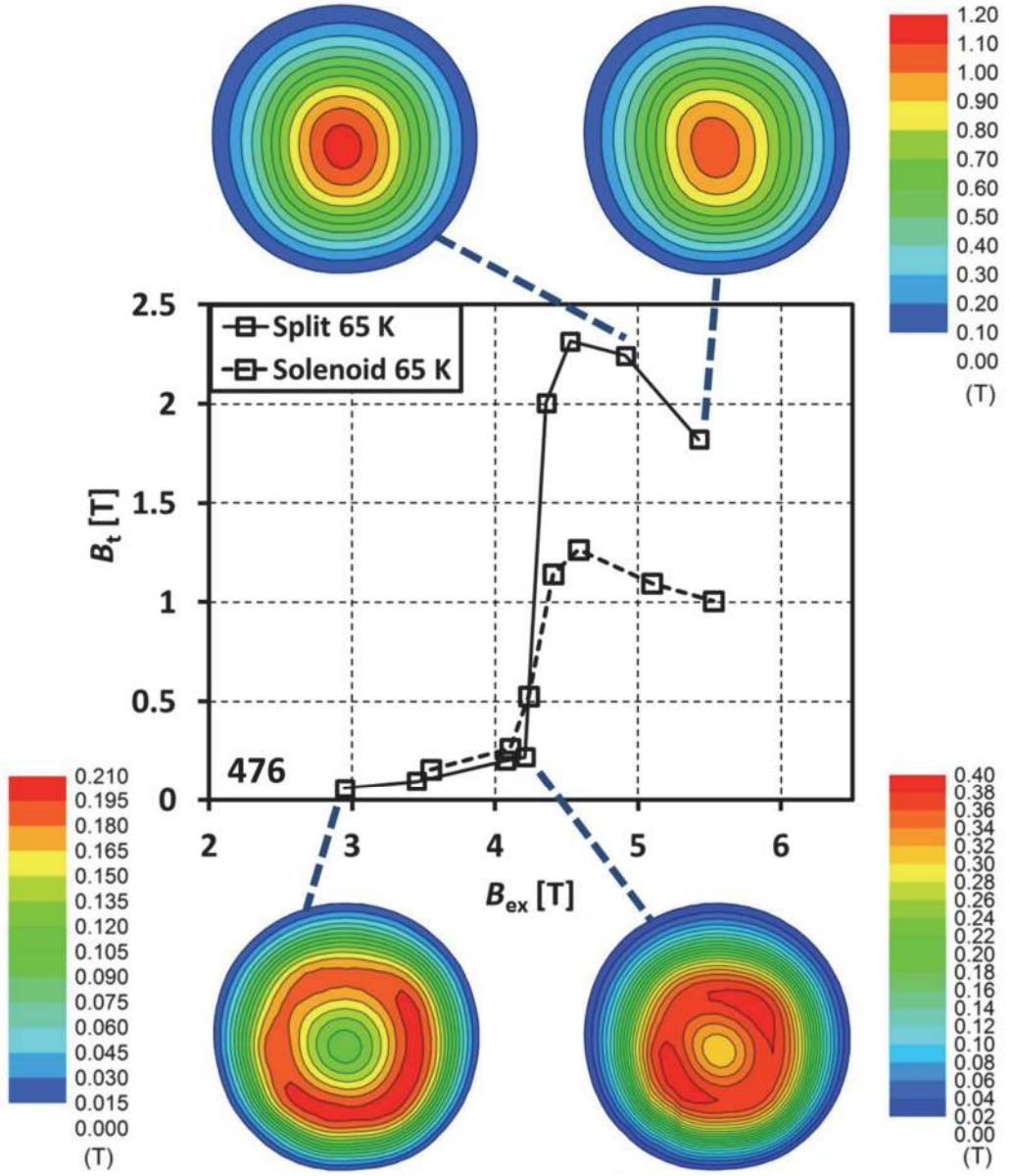

Figure 8. 2D trapped field profiles measured on the top surface (z = 2 mm) for sample #476 after PFM using the split coil with an iron yoke at an operating temperature of 65 K. The central panel shows the corresponding central trapped field, as shown in Figure 6.

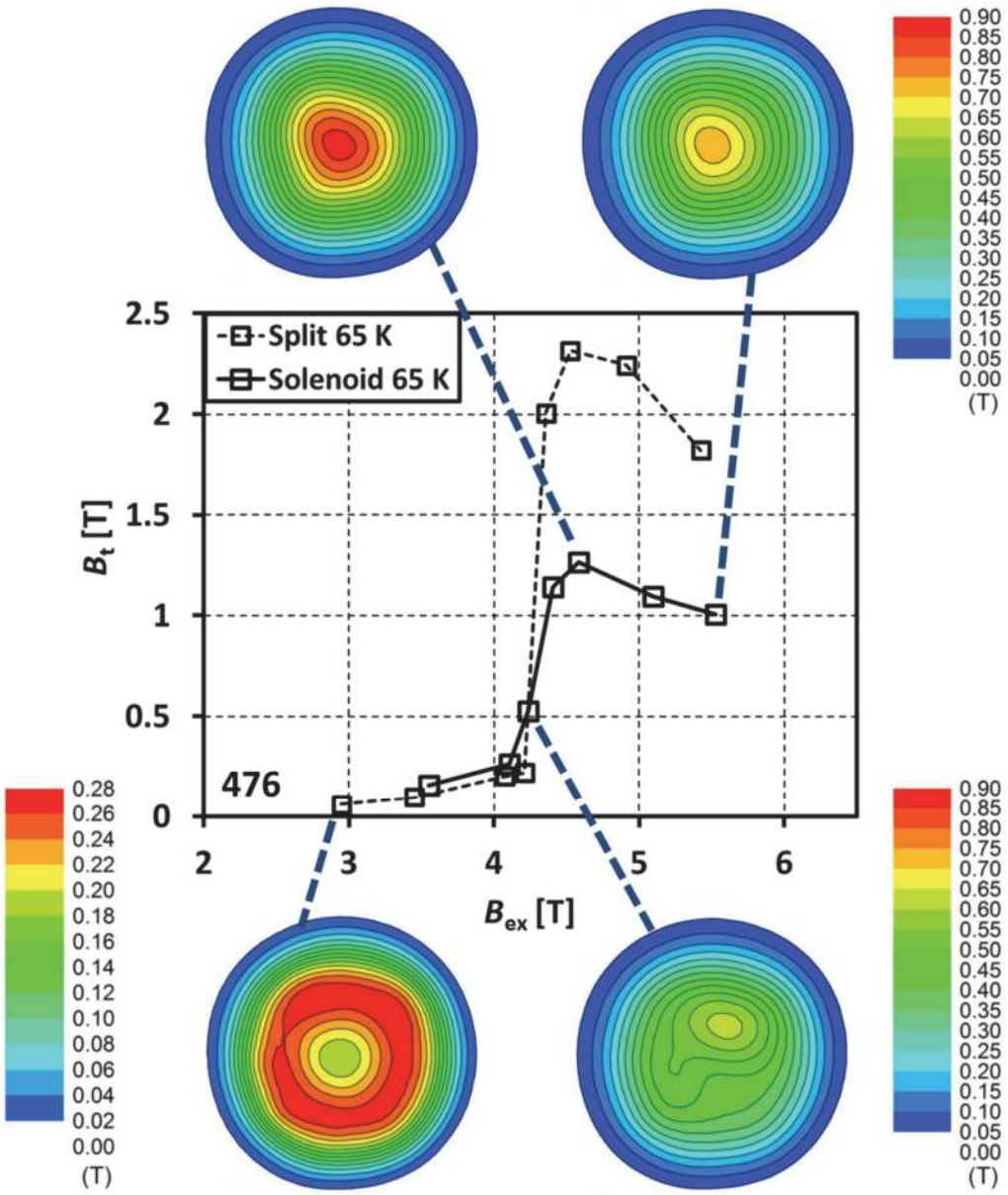

Figure 9. 2D trapped field profiles measured on the top surface (z = 2 mm) for sample #476 after PFM using the solenoid coil with an iron yoke at an operating temperature of 65 K. The central panel shows the corresponding central trapped field, as shown in Figure 6.

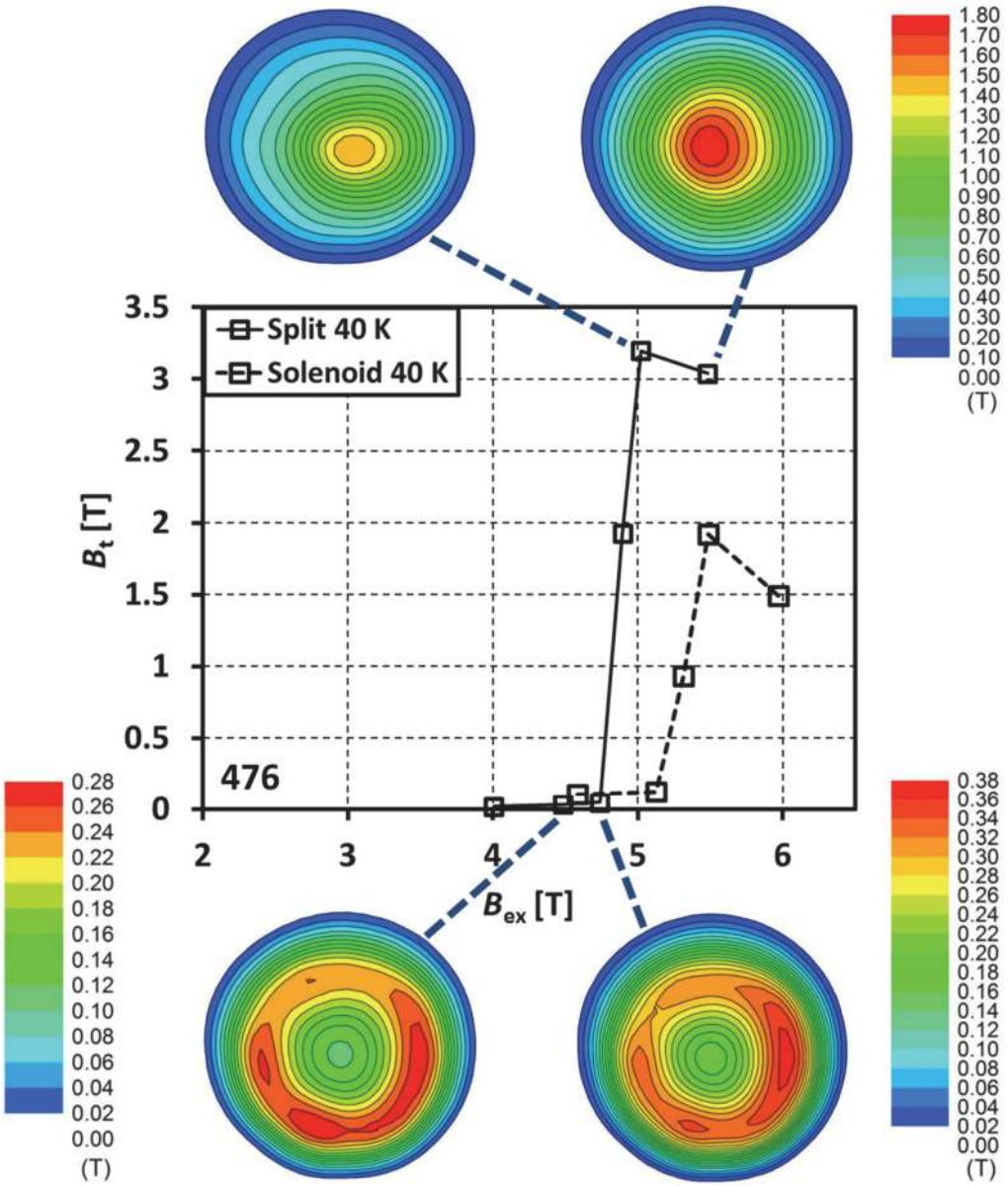

Figure 10. 2D trapped field profiles measured on the top surface (z = 2 mm) for sample #476 after PFM using the split coil with an iron yoke at an operating temperature of 40 K. The central panel shows the corresponding central trapped field, as shown in Figure 6.

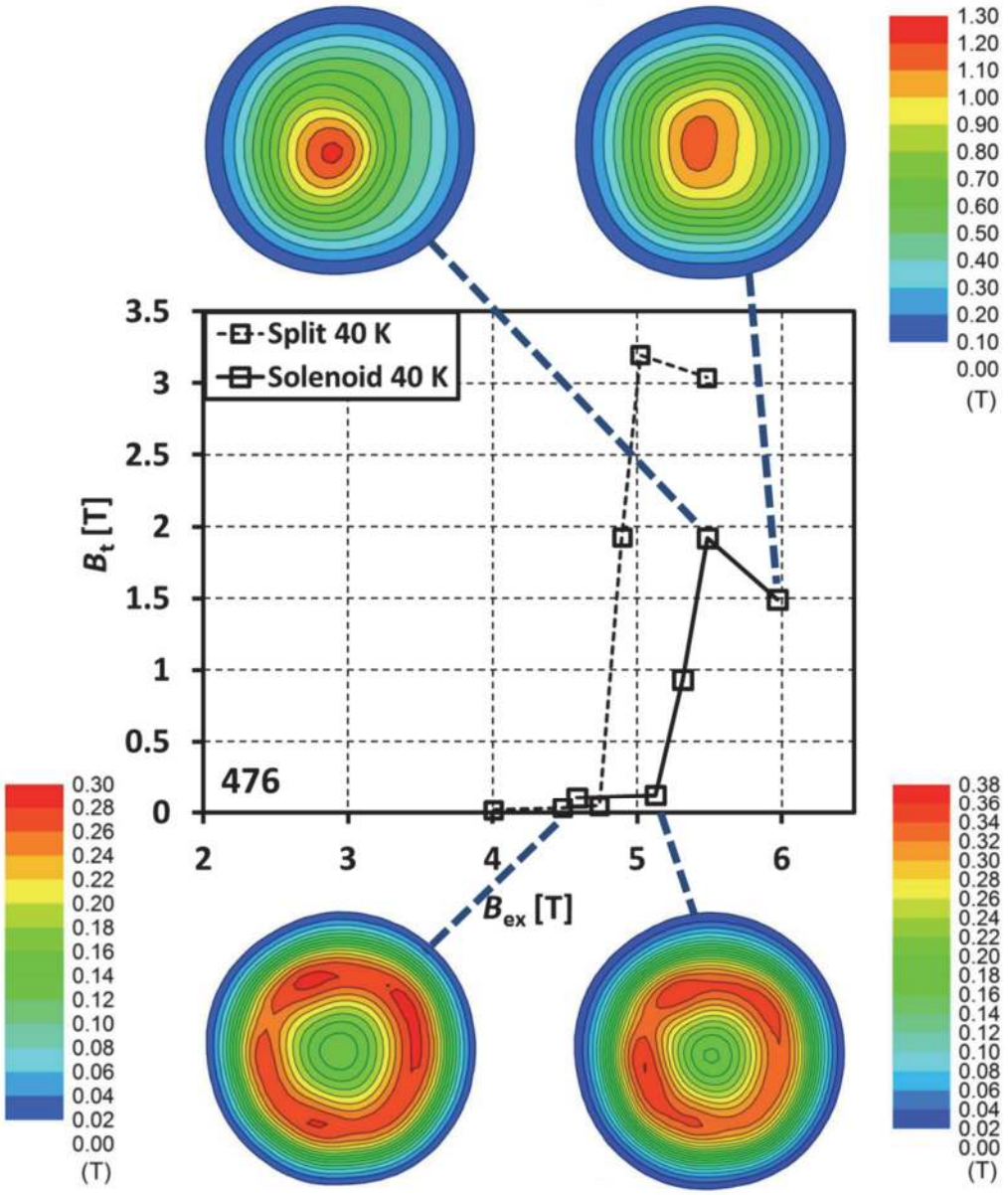

Figure 11. 2D trapped field profiles measured on the top surface (z = 2 mm) for sample #476 after PFM using the solenoid coil with an iron yoke at an operating temperature of 40 K. The central panel shows the corresponding central trapped field, as shown in Figure 6.

5. Numerical Modelling

5.1 Modelling Framework and Assumptions

The numerical model used here combines the electromagnetic and thermal equations governing the behaviour of the superconducting material, based on the 2D axisymmetric ***H***-formulation [22, 25, 28-31] implemented using the commercial FEM software package COMSOL Multiphysics 5.1. The general form, partial differential equation (PDE) interface of COMSOL is employed for the electromagnetic analysis and the Heat Transfer module is used for the thermal analysis, which are coupled together as described below and in [24].

In the 2D axisymmetric ***H***-formulation, the governing equations are derived from Maxwell's equations – namely, Faraday's (3) and Ampere's (4) laws:

$$\nabla \times \boldsymbol{E} + \frac{d\boldsymbol{B}}{dt} = \nabla \times \boldsymbol{E} + \frac{d(\mu_0 \mu_r \boldsymbol{H})}{dt} = 0 \qquad (1)$$

$$\nabla \times \boldsymbol{H} = \boldsymbol{J} \qquad (2)$$

where $\boldsymbol{H} = [H_r, H_z]$ represents the magnetic field components, $\boldsymbol{J} = [J_\phi]$ represents the current density and $\boldsymbol{E} = [E_\phi]$ represents the electric field. μ_0 is the permeability of free space and for all sub-domains other than the iron yoke (where present), the relative permeability is simply $\mu_r = 1$. For the iron yoke, the following equation [22, 31] is used to represent μ_r:

$$\mu_r = \mu_{r,\max} \text{ for } B < \mu_0 M_{sat},$$
$$\mu_r = (1 + \frac{M_{sat}}{H}) \text{ for } B \geq \mu_0 M_{sat} \qquad (3)$$

where $\mu_0 M_{sat}$ and $\mu_{r,max}$ are 1.6 T and 2000, respectively, as representative values for iron. The electrical properties of the superconductor are modelled using an *E-J* power law relation [32, 33], $E \alpha J^n$, where $n = 21$.

The results of the numerical model strongly depend on the $J_c(B, T)$ characteristics of the superconductor [12], and the experimental data for $J_c(B)$, measured between 30 – 85 K from a specimen taken from a representative bulk of the same composition as the two samples in this study (15 wt% Ag-containing GdBCO), is shown in Figure 12. The magnetic moment hysteresis (*m-H*) loops were measured using a Quantum Design Magnetic Property Measurement System XL SQUID magnetometer by applying the field parallel to the *c*-axis of the specimen and the variation of J_c with magnetic field was determined using the extended Bean model [34].

The experimental data (up to 4 T) is fit up to 10 T using equation (4) presented in [35] for samples exhibiting a fishtail shape in their magnetization loop. The coefficients related to the data fitting are shown in Table 1. This data is then input into the numerical model using a two-variable, direct interpolation, as described in [36, 37], where it is implemented for the

$J_c(B, \vartheta)$ data to model the complex anisotropy of high temperature superconducting (HTS) coated conductors in an HTS coil. This method of data input is simple and direct, and can significantly improve the computational speed of the model [36, 37].

$$J_c(B) = J_{c1} \exp\left(-\frac{B}{B_L}\right) + J_{c2} \frac{B}{B_{max}} \exp\left[\frac{1}{y}\left(1-\left(\frac{B}{B_{max}}\right)^y\right)\right] \quad (4)$$

Table 1. Data fitting coefficients for the $J_c(B)$ characteristics of a small sample using equation (4)

Temperature [K]	J_{c1}	B_L	J_{c2}	B_{max}	y
85	2.35e8	0.18	4.90e7	0.48	2.5
80	3.88e8	0.28	1.48e8	0.87	2
77	4.83e8	0.34	2.20e8	1.12	1.87
70	7.13e8	0.48	4.40e8	1.75	1.75
60	1.10e9	0.7	9.00e8	2.65	1.5
50	1.70e9	0.8	1.49e9	3.5	1.2
40	2.50e9	0.8	2.20e9	4.2	0.8
30	3.70e9	0.94	3.00e9	5.5	0.5

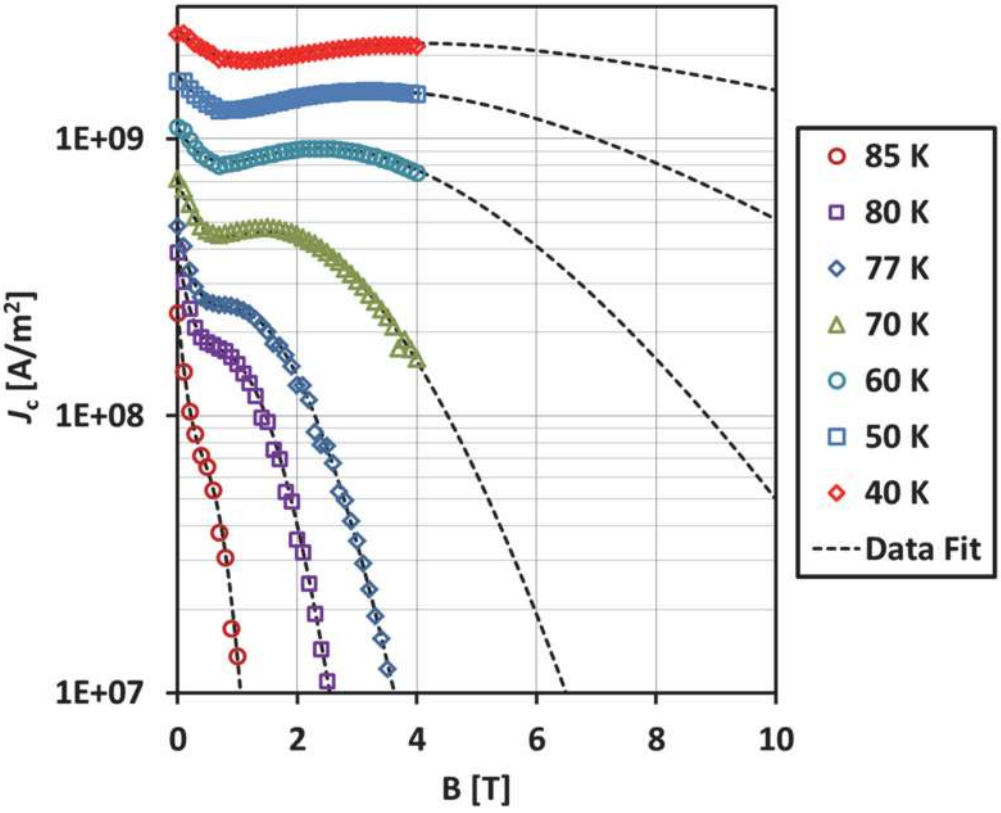

Figure 12. Experimental data for $J_c(B)$, measured from a small sample taken from a representative bulk of the same composition as the two samples (15 wt% Ag-containing Gd-Ba-Cu-O). The experimental data is fit up to 10 T using the equation presented in [35] for samples exhibiting a fishtail shape in their $J_c(B)$ curves.

To validate the $J_c(B)$ data, a ZFC process is employed to check the trapped field capability of a bulk sample [22, 38]. In this case, since the magnetization process is slow, isothermal conditions are assumed; hence, no thermal model is included. A magnetic field of magnitude at least twice the expected trapped field (based on the FC magnetization data in Figure 1) is applied using uniform boundary conditions at a slow ramp rate of 8 mT/s. It is found that the magnitude of $J_c(B)$ should be adjusted to one third of its small specimen value to adequately reproduce the FC magnetization results presented in Figure 1, resulting in B_t (77 K) = 1.12 T, B_t (70 K) = 1.94 T, B_t (60 K) = 3.67 T, and B_t (40 K) = 8.63 T (also shown for reference in Figure 1). Therefore, the overall pinning characteristics of the sample are maintained, while reproducing sensible and realistic trapped fields in the model.

Suitable parameters for the thermal properties must also be assumed for the materials and input into the model. The measured, temperature-dependent thermal conductivity data for the SUS ring and Stycast™ (2850GT) over the temperature range 0 – 100 K is shown in Figure 13, and the specific heat data for the SUS ring, Stycast™ (epoxy data from [39]), GdBCO and indium sheet [40] is shown in Figure 14. In the models, the operating temperature of the cold head, T_{op}, is set on the side of the indium sheet not connected to the bulk sample, as indicated in Figures 15 and 16 for the split and solenoid coil, respectively. These figures show the 2D axisymmetric model setups for the numerical simulations.

In previous work, the magnetizing field has been applied using uniform boundary conditions [24], but in this work, the field is applied via a pulse current applied to the magnetizing coils (copper coil subdomain). An integral constraint for the current is applied to the copper coil subdomain, as described in [36], using the following I_{pulse} function:

$$I_{pulse}(t) = N \cdot I_0 \frac{t}{\tau} \exp\left(1 - \frac{t}{\tau}\right) \quad (5)$$

where I_0 is the peak magnitude of the current flowing in each turn of the coil, N is the number turns, and τ is the rise time of the pulse (see Table 2). Table 2 also summarises the other assumed model parameters, including the thermal conductivity of the indium sheet, which is set to 0.5 W/mK to represent the finite cooling power of the refrigerator and the thermal contact between the bulk and the cold stage, as described in [41]. The rise time of the applied current, and hence resultant magnetic field, is the same value (τ = 15 ms) for all models in order to adequately compare pulsed fields of equivalent duration, magnitude and shape. The rise time is slightly different experimentally (see Fig. 5) due to a difference in the inductance of the coils.

Finally, Figure 17 shows the magnetic field at the centre of the magnetizing fixture, calculated using the numerical models with the bulk removed, for (a) solenoid coil with and without the iron yoke and (b) split coil with and without the iron yoke. This figure is then used a reference to apply particular pulsed fields with the bulk present, the results of which are analysed in the next section. An important result from Figure 17 is that the presence of

an iron yoke for both magnetizing coils results in a larger magnetic field at the centre of the fixture for the same applied current, reducing the requirements for the magnetizing fixture.

Table 2. Other assumed model parameters

PARAMETER	DESCRIPTION	VALUE
T_c	Superconducting transition temperature	92 K
T_{op}	Operating temperature (cold head)	40, 65 K
ρ_b	HTS bulk density	5.9 x 10^3 kgm^{-3}
k_{ab}	Thermal conductivity of bulk along ab-plane	20 $Wm^{-1}K^{-1}$
k_c	Thermal conductivity of bulk along c-axis	4 $Wm^{-1}K^{-1}$
k_{indium}	Artificial thermal conductivity of indium sheet	0.5 $Wm^{-1}K^{-1}$
E_0	Characteristic voltage	1 x 10^{-4} Vm^{-1}
τ	Rise time of applied pulsed current/magnetic field	15 ms

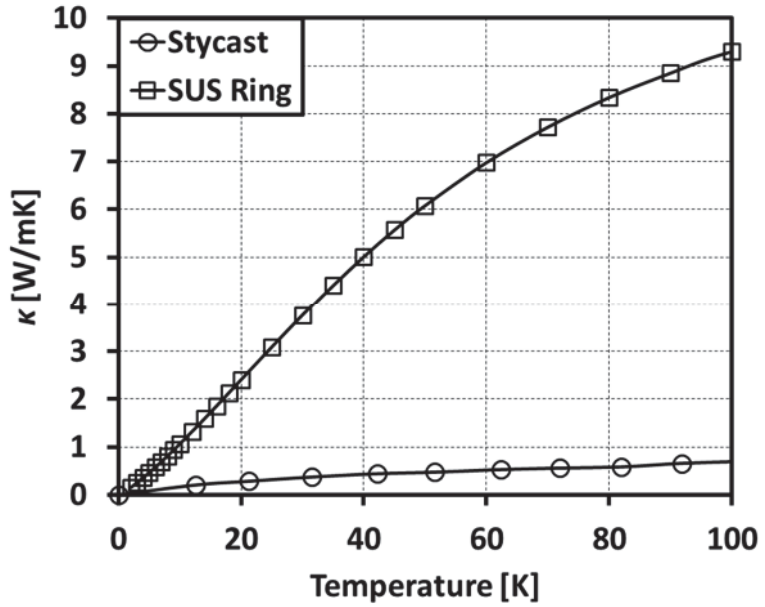

Figure 13. Measured, temperature-dependent thermal conductivity data for Stycast™ (2850GT) and SUS for the numerical models.

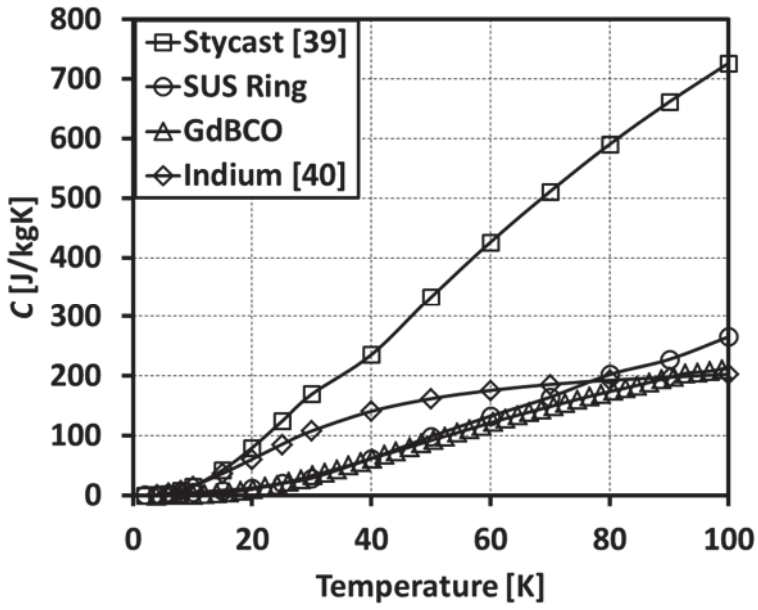

Figure 14. Measured, temperature-dependent specific heat data for Stycast™ (epoxy data from [39]), SUS, GdBCO with 15 wt% Ag and indium [40] for the numerical models.

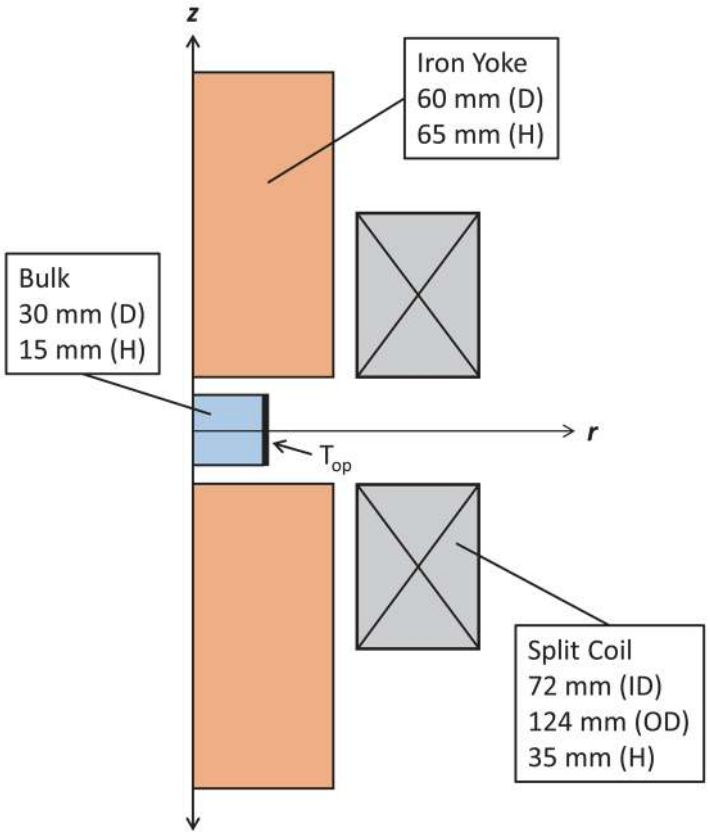

Figure 15. 2D axisymmetric model setup for numerical simulation of the split coil with an iron yoke. A thin (0.2 mm) indium sheet is placed around the bulk to provide a good thermal contact to the sample holder.

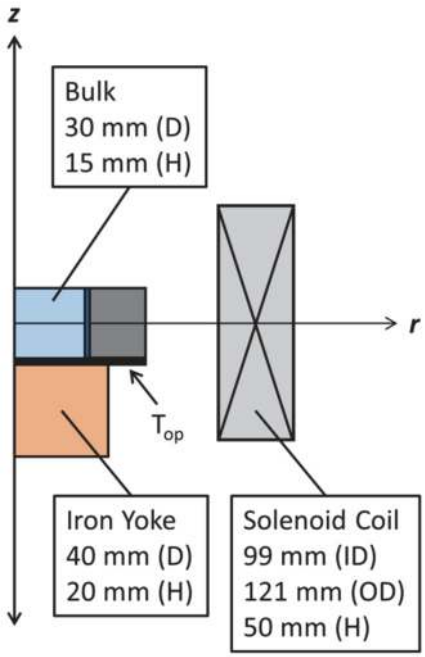

Figure 16. 2D axisymmetric model setup for numerical simulation of the solenoid coil with an iron yoke. A thin (0.2 mm) indium sheet is placed between the bulk and cold stage to provide a good thermal contact. The bulk is embedded in a SUS ring using Stycast™ (2850GT).

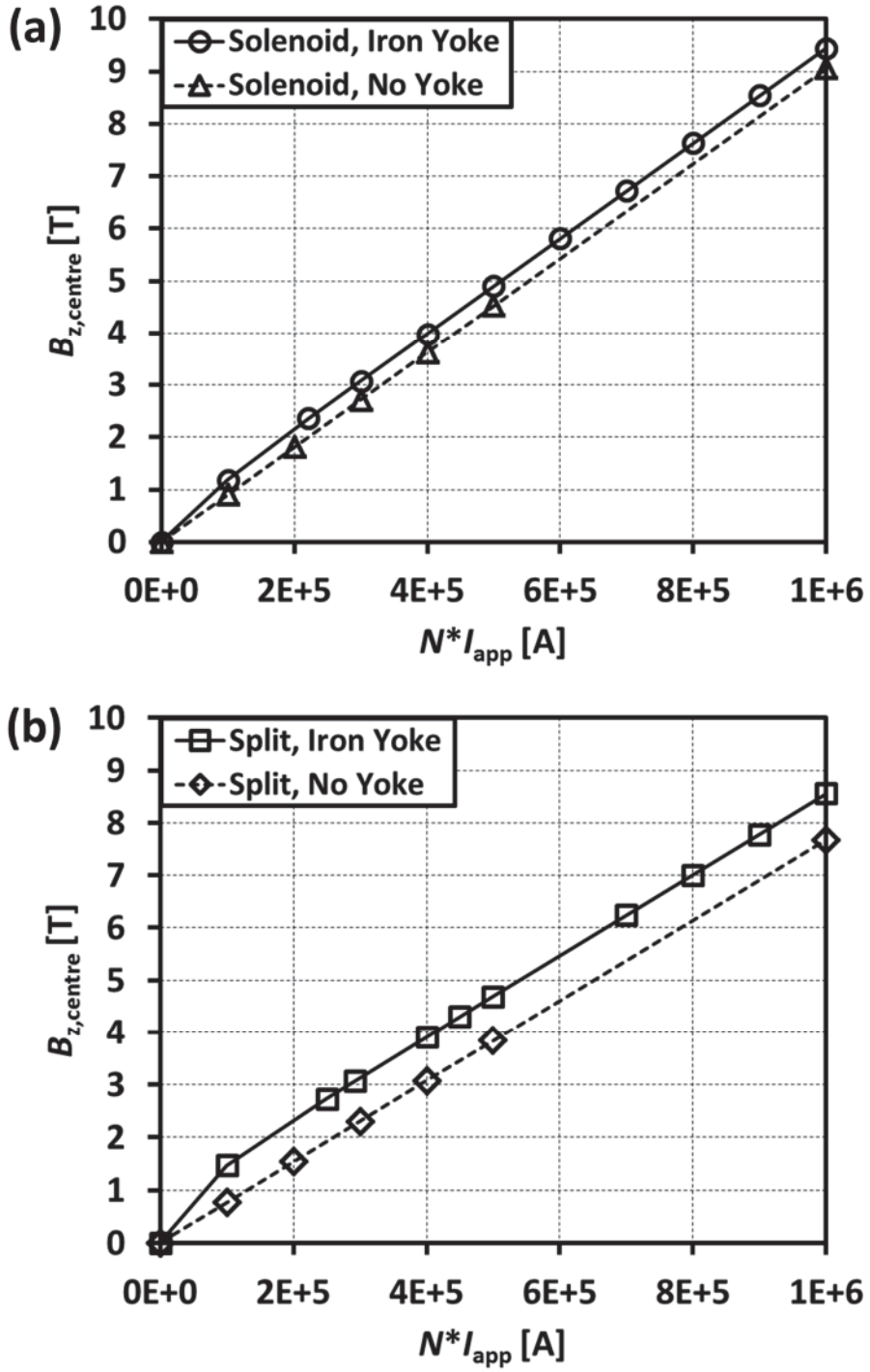

Figure 17. Magnetic field at the centre of the magnetizing fixture at the peak of the pulsed current, calculated using the numerical models with the bulk removed, for (a) solenoid coil with and without the iron yoke and (b) split coil with and without the iron yoke.

5.2 Numerical Results and Discussion

Figure 18 shows the trapped magnetic field at the centre of the top surface of the bulk sample (r = 0 mm) at a height of 0.1 mm at t = 300 ms for the split and solenoid coils with and without the iron yoke for two temperatures: (a) T_{op} = 65 K and (b) T_{op} = 40 K. In comparison to the case where no yoke is present, the presence of the iron yoke clearly enhances the calculated trapped field, and this enhancement is particularly pronounced for the split coil, qualitatively reproducing the experimental results shown in Figures 6 and 7 (also measured at $t \approx$ 300 ms). In the case of no yoke present, the split and solenoid coil arrangements see essentially the same trapped field at both temperatures. The average temperature, T_{ave}, of the bulk, is shown in Figure 19 as calculated at t = 300 ms for all cases for (a) T_{op} = 65 K and (b) T_{op} = 40 K. There is no significant difference in the average temperature of the bulk, and the presence of the iron yoke slightly reduces the temperature rise in both cases.

The measured trapped fields shown in Figures 6 and 7 were measured before the split coil and yoke were removed for the 2D surface plot scanning measurement, and hence, the presence of the yoke would be expected to enhance the locally measured magnetic field. This results in the observed reduction in trapped field when analysing the 2D surface plots, which are also measured approximately 20 mins after the application of the pulse. In order to assess the 'true' trapped field, with the split coil and iron yoke removed, Figures 20(a) and 21(a) show the evolution of the trapped field from t = 300 ms (corresponding to the calculated trapped fields shown in Figure 18) to t = 10 s, after removing the iron yoke from the split coil at t = 4 s. Here we examine two particular cases, both of which correspond to the maximum trapped field cases seen in Figure 18: 1) T_{op} = 65 K, B_{ex} = 4 T, and 2) T_{op} = 40 K, B_{ex} = 6.5 T.

The removal of the iron yoke is simulated by reducing the $\mu_0 M_{sat}$ value exponentially to zero with a time constant of 20 ms, i.e., an $exp(-t/0.02)$ function, resulting in an equivalent permeability of the iron yoke of μ_0 (μ_r = 1) after a period of several time constants. The dashed line in Figures 20(a) and 21(a) show the calculated trapped field when the yoke is removed at t = 4 s. For both temperatures, there is a reduction in the observed trapped field when the yoke is removed – at 40 K, the difference is almost negligible – but the trapped field is still higher than in the case of the solenoid coil with the yoke, where the yoke remains embedded in the fixture.

Another important consideration is the average temperature rise during the entire magnetization process and subsequent cooling rate for each magnetizing fixture. Figures 20(b) and 21(b) show the calculated T_{ave} in the bulk as the pulse increases t = 2, 4, 6, 8, 10 and 15 ms (pulse peak), followed by t = 30, 100, 300 ms, 1, 3, 5 and 10 s. Similar to Figure 19 (calculated only at t = 300 ms), the temperature rise during the application of the pulse is very similar for both the split and solenoid coils with the yoke, but the bulk cools back down to T_{op} at a faster rate in the case of the split coil arrangement because the bulk is cooled

from the periphery through the *ab*-plane, for which the thermal conductivity is several times higher. Hence, the field decays slightly faster with time in the case of the solenoid coil. The same temperature profile is observed for the split coil whether or not the yoke is present for both T_{op} cases.

The numerical simulation can also provide an easy way of examining the flux penetration into the bulk and its subsequent exit from the sample as the pulse reduces to zero, which is extremely difficult to achieve experimentally. Figure 22(a) shows the flux penetration into the sample (t = 2, 4, 6, 8, 10 and 15 ms) for T_{op} = 65 K, B_{ex} = 4 T as the pulse reaches its peak value (t = 15 ms). The values plotted are for B_z across the middle of the bulk from the edge to the centre. The iron yoke acts to improve flux penetration initially, but at the pulse peak, a similar flux penetration is observed. As the pulse reduces and the bulk cools back down towards T_{op}, the iron yoke acts to attract flux to remain in the bulk, as shown in Figure 22(b), for t = 30, 100, 300 ms, 1, 10 s. Significantly less flux exits the bulk when the iron core is present, resulting in a higher peak trapped field, as well as more overall trapped flux, after the magnetization process is complete. Figure 23 shows the results for the T_{op} = 40 K, B_{ex} = 6.5 T case and a similar trend is observed for both flux entry and exit.

For the solenoid coil, the enhancement of the field in comparison to no yoke can be attributed to both the difference in the flux exiting the bulk and the enhancement effect described in [22] from the presence of a ferromagnetic material on the bottom of the bulk, since the iron yoke is embedded in the magnetizing fixture and cannot be removed after the magnetization process.

The experimental results, which have been verified by numerical simulation, have important implications for practical applications of bulk superconductors. Such a split coil arrangement with an iron yoke could be incorporated into the design of a portable, high magnetic field source/magnet to enhance the available magnetic field. It also has strong implications for an axial gap-type bulk superconducting electric machine, where iron can be incorporated into the stator windings to 1) improve the trapped field from the magnetization process, and 2) increase the effective air-gap magnetic field.

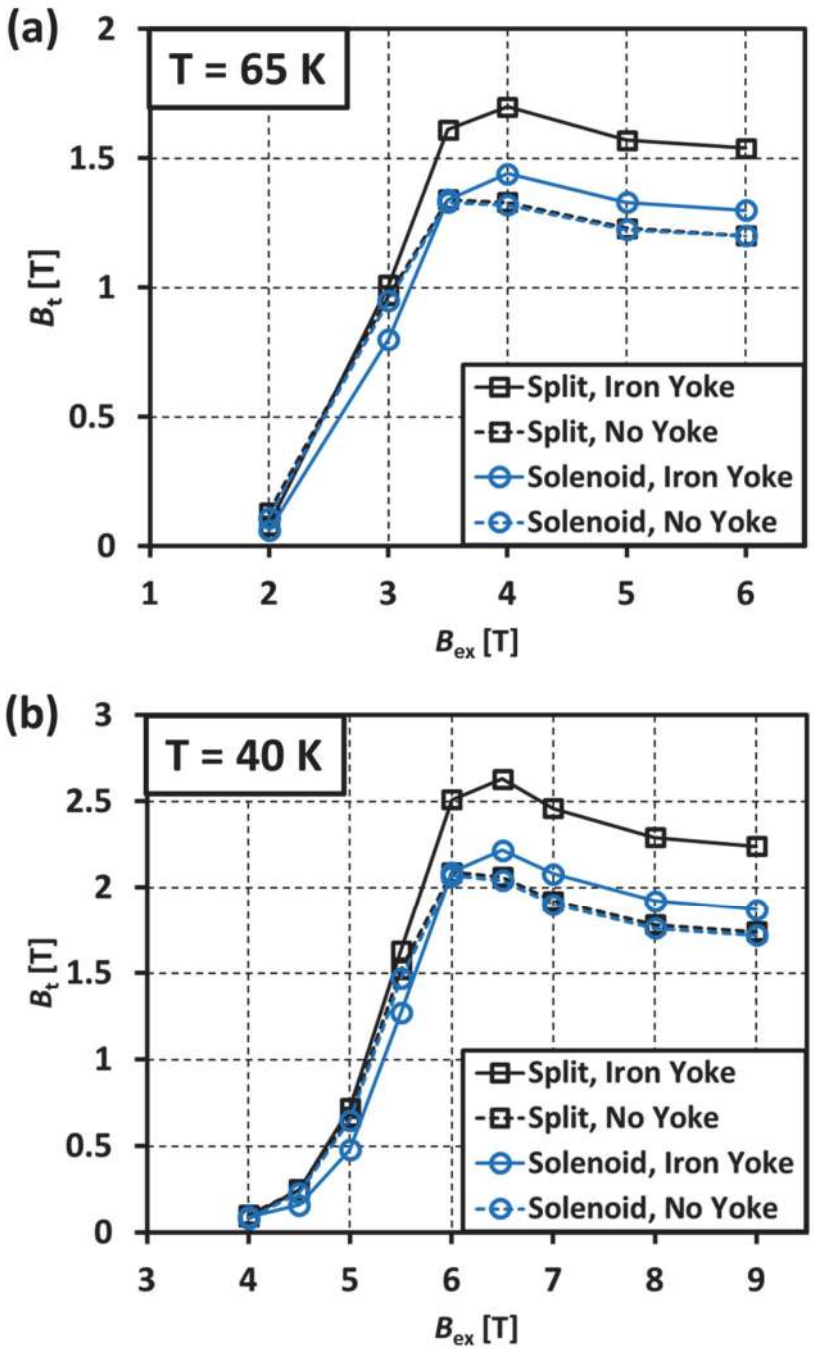

Figure 18. Numerical simulation results for the trapped magnetic field at the centre of the top surface of the bulk sample (r = 0 mm) at a height of 0.1 mm at t = 300 ms for the split and solenoid coils with and without the iron yoke for two temperatures: (a) T_{op} = 65 K and (b) T_{op} = 40 K.

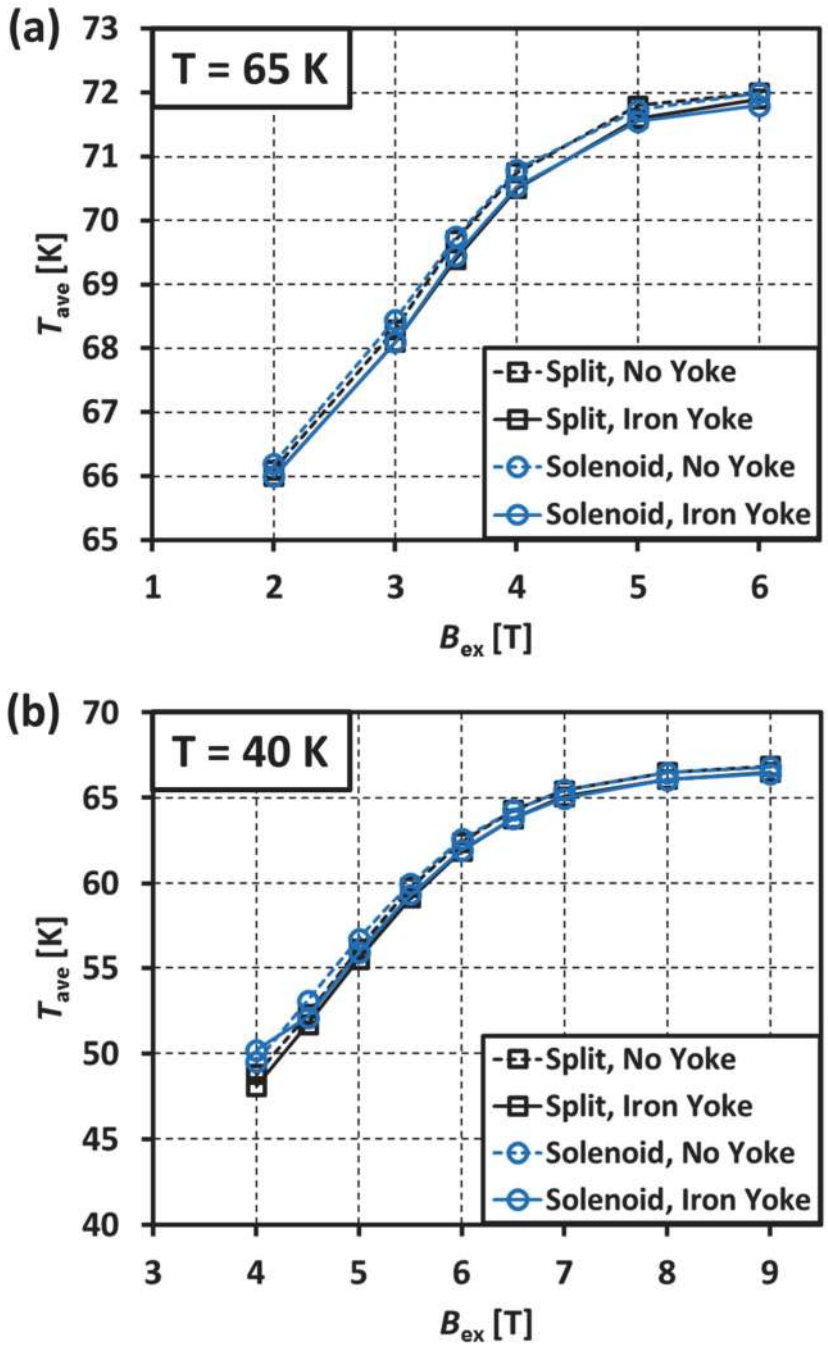

Figure 19. Numerical simulation results for the average temperature of the bulk, T_{ave}, at t = 300 ms for the split and solenoid coils with and without the iron yoke for two temperatures: (a) T_{op} = 65 K and (b) T_{op} = 40 K.

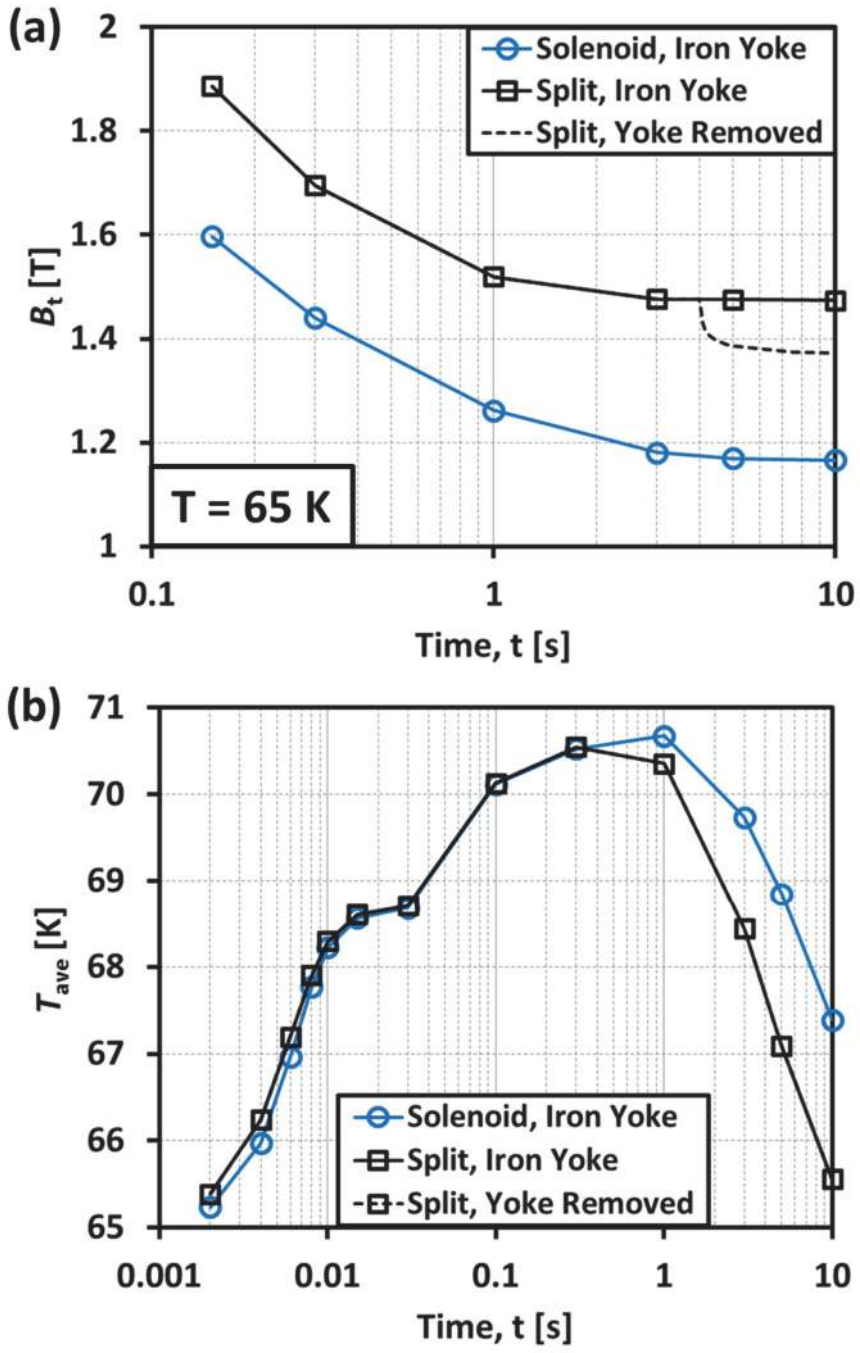

Figure 20. Evolution of the (a) trapped field and (b) average temperature, T_{ave}, from t = 300 ms (corresponding to the calculated trapped fields shown in Figure 18) to t = 10 s for the split and solenoid coil with an iron yoke, including the case where the iron yoke is removed from the split coil at t = 4 s. This particular case corresponds to T_{op} = 65 K, B_{ex} = 4 T, which resulted in the maximum trapped field in Figure 18(a).

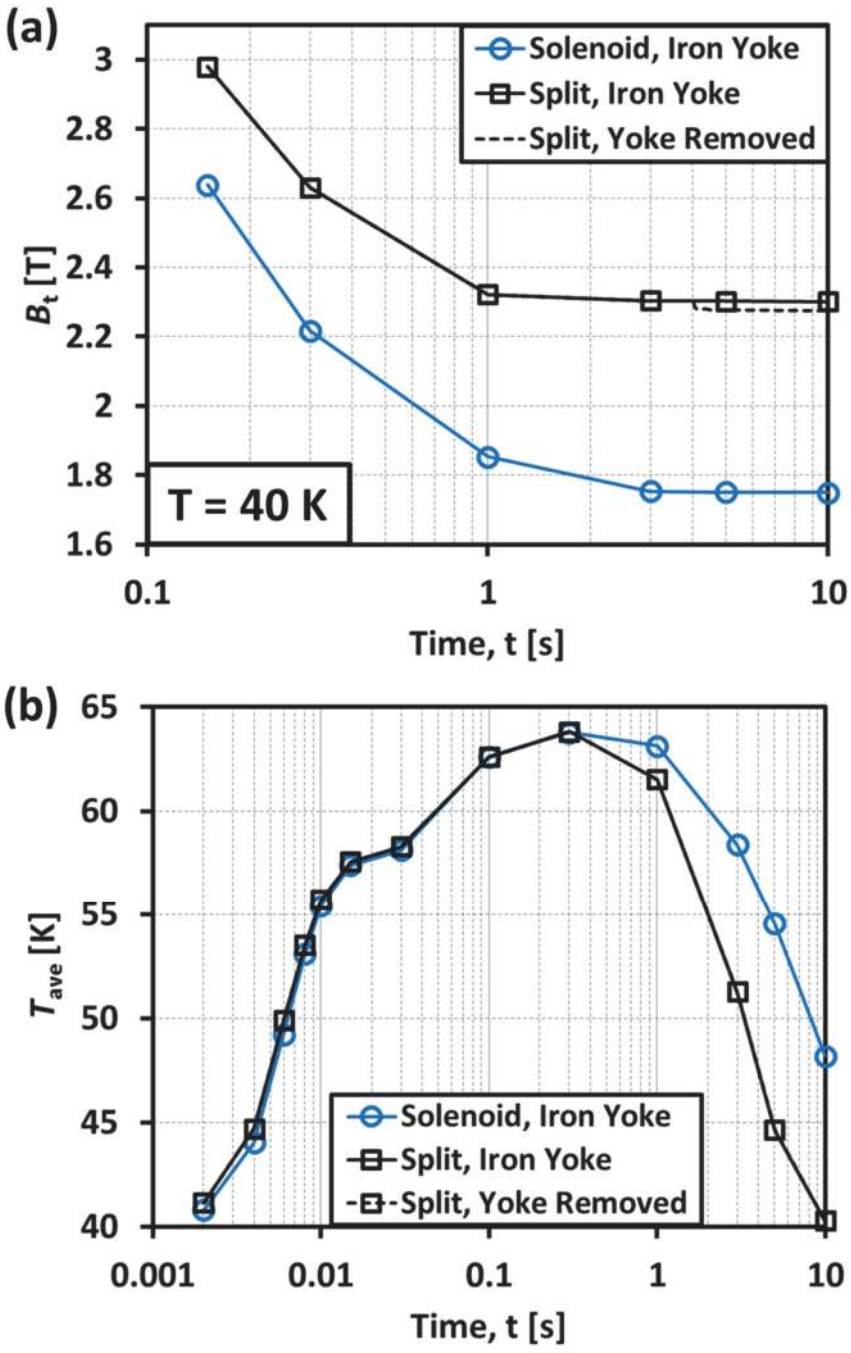

Figure 21. Evolution of the (a) trapped field and (b) average temperature, T_{ave}, from t = 300 ms (corresponding to the calculated trapped fields shown in Figure 18) to t = 10 s for the split and solenoid coil with an iron yoke, including the case where the iron yoke is removed from the split coil at t = 4 s. This particular case corresponds to T_{op} = 40 K, B_{ex} = 6.5 T, which resulted in the maximum trapped field in Figure 18(b).

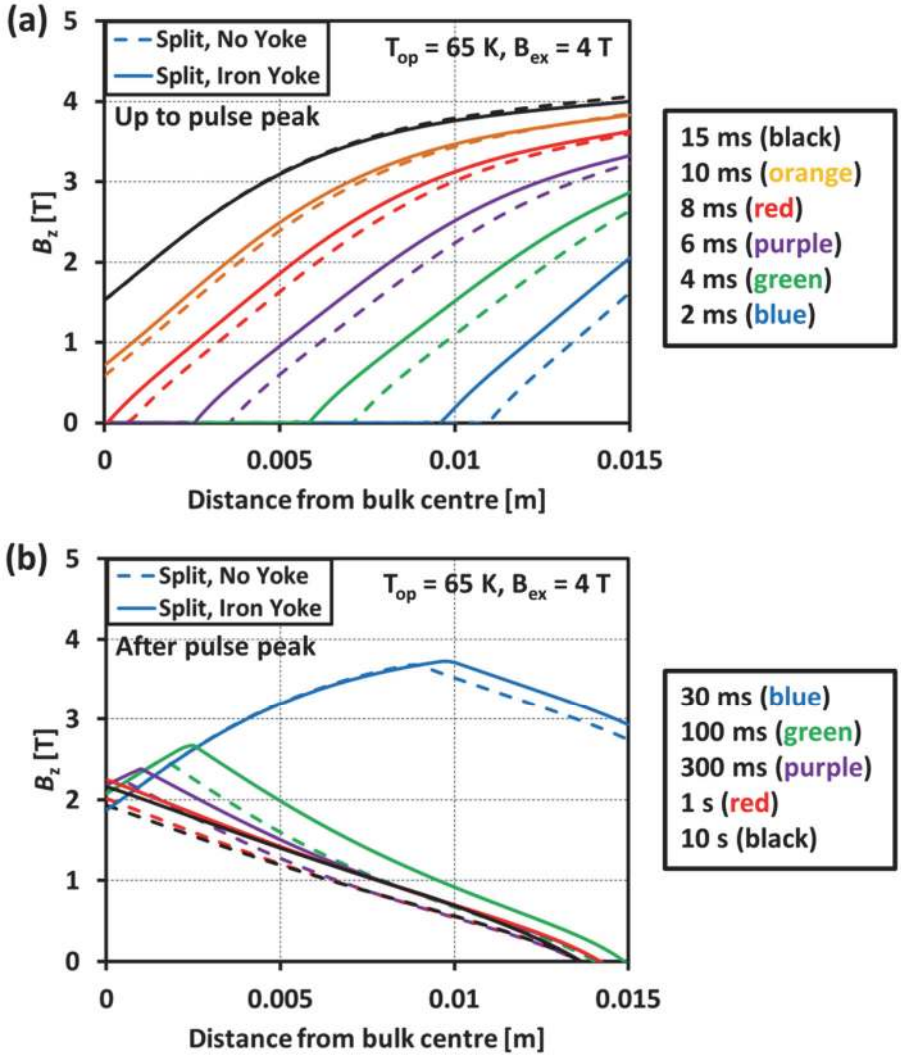

Figure 22. (a) Flux penetration into the sample for T_{op} = 65 K, B_{ex} = 4 T, for the split coil with and without an iron yoke, at t = 2 ms (blue), 4 ms (green), 6 ms (purple), 8 ms (red), 10 ms (orange) and 15 ms (black). The pulse reaches its peak value at t = 15 ms. (b) Flux exiting the sample as the pulse reduces and the bulk cools back down towards T_{op} at t = 30 ms (blue), 100 ms (green), 300 ms (purple), 1 s (red) and 10 s (black).

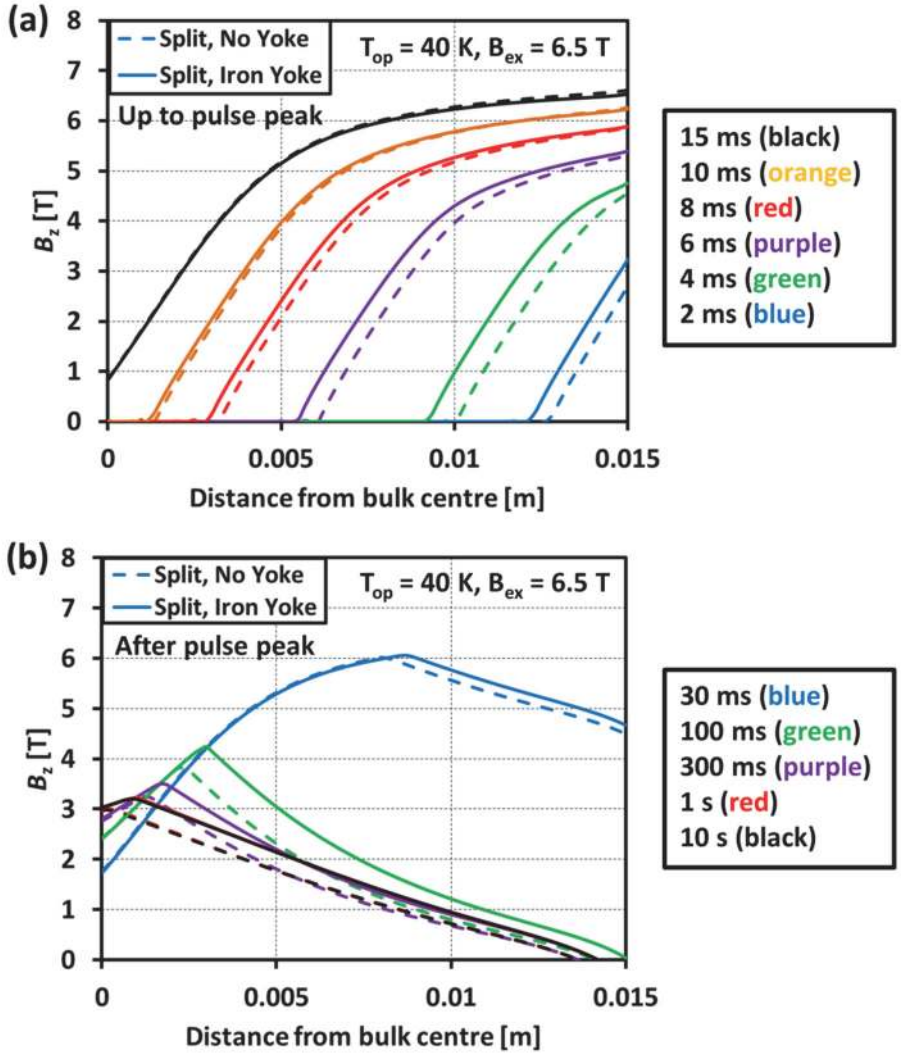

Figure 23. (a) Flux penetration into the sample for T_{op} = 40 K, B_{ex} = 6.5 T, for the split coil with and without an iron yoke, at t = 2 ms (blue), 4 ms (green), 6 ms (purple), 8 ms (red), 10 ms (orange) and 15 ms (black). The pulse reaches its peak value at t = 15 ms. (b) Flux exiting the sample as the pulse reduces and the bulk cools back down towards T_{op} at t = 30 ms (blue), 100 ms (green), 300 ms (purple), 1 s (red) and 10 s (black).

6. Conclusion

In this paper, the PFM of two, standard Ag-containing Gd-Ba-Cu-O samples – of the same composition that recently achieved the new record trapped field – is carried out using two types of magnetizing coils with an iron yoke: a solenoid coil and a split coil arrangement. A significantly higher trapped field can be achieved using a split coil with an iron yoke, and in order to explain these how this arrangement works in detail, numerical simulations using a 2D axisymmetric finite element method based on the ***H***-formulation are carried to qualitatively reproduce and analyse the magnetization process from both electromagnetic and thermal points of view. During PFM, the iron yoke in the split coil acts to improve flux penetration initially, but at the pulse peak, a similar flux penetration is observed. However, as the pulse reduces and the bulk cools back down towards the operating temperature, T_{op}, the iron yoke acts to attract flux to remain in the bulk. Significantly less flux exits the bulk when the iron core is present, resulting in a higher peak trapped field, as well as more overall trapped flux, after the magnetization process is complete. The results have important implications for practical applications of bulk superconductors as such a split coil arrangement with an iron yoke could be incorporated into the design of a portable, high magnetic field source/magnet to enhance the available magnetic field or in an axial gap-type bulk superconducting electric machine, where iron can be incorporated into the stator windings to 1) improve the trapped field from the magnetization process, and 2) increase the effective air-gap magnetic field.

Acknowledgments

Mark Ainslie would like to acknowledge the support of a Royal Academy of Engineering Research Fellowship. Hiroyuki Fujishiro would like to acknowledge support in part by a Grant-in-Aid for Scientific Research from the Ministry of Education, Culture, Sports, Science and Technology, Japan. This research was also supported in part by a Royal Society International Exchanges Scheme grant, IE131084. Jin Zou would like to acknowledge the support of Churchill College, Cambridge, the China Scholarship Council and the Cambridge Commonwealth, European and International Trust.

References

[1] Campbell A M and Cardwell D A 1997 *Cryogenics* **37** 567–75

[2] Tomita M and Murakami M 2003 *Nature* **421** 517–20

[3] Durrell J H *et al* 2014 *Supercond. Sci. Technol.* **27** 082001

[4] Nariki S, Sakai N and Murakami M 2005 *Supercond. Sci. Technol.* **18** S126–30

[5] Hull J and Murakami M 2004 *Proc. IEEE* **92** 1705–18

[6] Murakami M 2007 *Int. J. Appl. Ceram. Technol.* **4** 225–41

[7] Li B *et al* 2012 *Phys. C: Supercond.* **482** 50–7

[8] Granados X *et al* 2008 *Supercond. Sci. Technol.* **21** 034010

[9] Ainslie M D *et al* 2010 *Phys. C: Supercond.* **470** 1752-1755

[10] Zhou D *et al* 2012 *Supercond. Sci. Technol.* **25** 103001

[11] Ainslie M D et al 2014 *J. Phys.: Conf. Ser.* **507** 032002

[12] Ainslie M D and Fujishiro H 2015 *Supercond. Sci. Technol.* **28** 053002

[13] Fujishiro H, Tateiwa T, Fujiwara A, Oka T and Hayashi H 2006 *Phys. C: Supercond.* **445–48** 334–8

[14] Granados X, Torner M, Puig T and Obradors X 2007 *IEEE Trans. Appl. Supercond.* **17** 1629–32

[15] Hull J R and Strasik M 2010 *Supercond. Sci. Technol.* **23** 124005

[16] Takao T, Tanoue N, Kameyama S, Doi T and Kamijo H 2012 *IEEE Trans. Appl. Supercond.* **22** 3600404

[17] Takao T, Horie T, Usami T, Takahashi M and Kamijo H 2014 *IEEE Trans. Appl. Supercond.* **24** 3600504

[18] Ikuta H, Ishihara H, Yanagi Y, Itoh Y and Mizutani U 2002 *Supercond. Sci. Technol.* **15** 606–12

[19] Parks D, Weinstein R, Davey K, Sawh R P and Mayes B W 2009 *IEEE Trans. Appl. Supercond.* **19** 2937–40

[20] Philippe M P *et al* 2014 *Phys. C: Supercond.* **502** 20–30

[21] Gony B *et al* 2015 *IEEE Trans. Appl. Supercond.* **25** 8801005

[22] Philippe M P *et al* 2015 *Supercond. Sci. Technol.* **28** 095008

[23] Shi Y *et al* 2010 *Phys. C: Supercond.* **470** 685–8

[24] Ainslie M D *et al* 2014 *Supercond. Sci. Technol.* **27** 065008

[25] Zou J *et al Supercond. Sci. Technol.* **28** 075009

[26] Ainslie M D *et al* 2015 *Supercond. Sci. Technol.* **28** 125002

[27] Withnell T D, Hari-Babu N, Ganney I, Dennis A and Cardwell D A 2008 *Mater. Sci. Eng. B* **151** 79–83

[28] Zhang M, Kvitkovic J, Pamidi S V and Coombs T A 2012 *Supercond. Sci. Technol.* **25** 125020

[29] Patel A and Glowacki B A 2012 *Supercond. Sci. Technol.* **25** 125015

[30] Zou J, Ainslie M D, Hu D and Cardwell D A 2015 *IEEE Trans. Appl. Supercond.* **25** 4900505

[31] Zou J, Ainslie M D, Hu D and Cardwell D A 2016 *IEEE Trans. Appl. Supercond.* **26** 8200605

[32] Plummer C J G and Evetts J E 1987 *IEEE Trans. Magn.* **23** 1179-82

[33] Rhyner J 1993 *Physica C* **212** 292-300

[34] Chen D X and Goldfarb R B 1989 *J. Appl. Phys.* **66** 2489–500

[35] Jirsa M, Půst L, Dlouhý D and Koblischka M R 1997 *Phys. Rev. B* **55** 3276–84

[36] Hu D *et al* 2015 *Supercond. Sci. Technol.* **28** 065011

[37] Hu D *et al* 2016 *IEEE Trans. Appl. Supercond.* **26** 6600906

[38] Zou J *et al* 2015 *Supercond. Sci. Technol.* **28** 035016

[39] Iwasa Y 2009 *Case Studies in Superconducting Magnets: Design and Operational Issues* (New York, USA: Springer Science+Business Media, LLC) pp 354–5

[40] Jensen J E et al 1980 *Brookhaven National Laboratory Selected Cryogenic Data Notebook*, Vol. I, Section VIII: Specific Heat of Some Solids pp VIII-C-3

[41] Fujishiro H *et al* 2011 *Supercond. Sci. Technol.* **24** 105003